RSC Advances

PAPER

View Article Online
View Journal | View Issue

CrossMark click for updates

Cite this: RSC Adv., 2016, 6, 38563

Fullerenol nanoparticles as a new delivery system for doxorubicin†

Danica S. Jović,‡[a] Mariana N. Seke,‡[b] Aleksandar N. Djordjevic,*[a] Jasminka Ž. Mrđanović,[c] Lidija D. Aleksić,[c] Gordana M. Bogdanović,[c] Aleksandar B. Pavić[d] and Janez Plavec[e]

Doxorubicin is a very potent chemotherapeutic drug, however its side effects limit its clinical use. The aim of this research was to investigate the properties of a fullerenol/doxorubicin nanocomposite, its potentially cytotoxic and genotoxic effects on malignant cell lines, as well as its toxicity towards zebra fish embryos. Chromatographic, NMR and mass spectral analysis of the nanocomposite imply that interactions between doxorubicin and fullerenol are non-covalent bonds. The stability of the nanocomposite was confirmed by the use of atomic force microscopy, dynamic light scattering and transmission electron microscopy. The nanocomposite, compared to the free doxorubicin at equivalent concentrations, significantly decreased the viability of MCF-7 and MDA-MB-231 cells. The flow cytometry results indicated that doxorubicin-loaded fullerenol could remarkably increase the uptake of doxorubicin suggesting that fullerenol might be a promising intracellular targeting carrier for the efficient delivery of antitumor drugs into tumor cells. The nanocomposite also affected cell cycle distribution. A genotoxicity test showed that the nanocomposite at all examined concentrations on MCF-7 and at lower concentrations on MDA-MB-231 cells caused DNA damage. Consequently, cell proliferation was notably reduced when compared with controls. Results of the zebrafish embryotoxicity assay showed a decreased overall toxicity, particularly cardiotoxicity and increased safety of the nanocomposite in comparison to doxorubicin alone, as manifested by a higher survival of embryos and less pericardial edema.

Received 11th February 2016
Accepted 13th April 2016

DOI: 10.1039/c6ra03879d

www.rsc.org/advances

Published on 14 April 2016. Downloaded by National Library of Serbia on 13/03/2018 11:39:29.

Introduction

Anthracyclines are highly effective and widely used antineoplastic agents in clinical practice. However, the main limiting factors of their application are multiple drug resistance and reduction in left ventricular function causing cardiomyopathy.[1–3] The major target of anticancer drugs such as doxorubicin (DOX) is topoisomerase II (TOP2).[4] DOX binds to DNA and TOP2 forming a TOP2–DOX–DNA cleavage complex that triggers cell death.[5] Furthermore, DOX activates p53 and induces apoptosis through transcriptional upregulation of Bax. Mutations that interfere with p53 function have been associated with resistance to anthracycline-based therapy.[6] Many previous studies have reported that oxidative stress was mainly responsible for DOX-induced cardiac gene dysregulation. Stress caused by oxidation/reduction affected redox cascades and initiated cell changes leading to cell damages and/or aberrant signaling and consequently causing cardiovascular disease, atherosclerosis, diabetes, cancer, inflammation, and apoptosis.[7] Additionally, individual transition metals have very important role in cell homeostasis. Many cardiovascular alterations as well as tumorigenesis in multiple human cancer types are connected with iron equilibrium in physiological processes.[8,9] Inside the cells, iron(III) and DOX can form a complex that goes through autoxidation under aerobic conditions.[10] These reactions could cause oxidative stress which can leads to mitochondrial dysfunction resulting in apoptosis. Iron chelators such as dexrazoxane (ICRF-187) is the only clinically approved drug in antharcycline-induced cardiomyopathy.[11] Nanoformulations of drugs have proven to be a positive solution for these problems. To date, there have been developed numerous nanodelivery systems for doxorubicin (DOX) based on: liposomes, polymeric micelles, peptide conjugates, solid-lipids, cyclodextrin, magnetic, gold, silica, and carbon nanoparticles.[2,11–13] In clinical practice, nanoformulations of DOX that are in use are *N*-(2-hydroxypropyl)methacrylamide (HPMA)-DOX and Doxil®,[14–16]

[a]Department of Chemistry, Biochemistry and Environmental Protection, Faculty of Sciences, University of Novi Sad, Novi Sad, Serbia. E-mail: aleksandar.djordjevic@dh.uns.ac.rs

[b]Institute of Nuclear Sciences "Vinča", University of Belgrade, Belgrade, Serbia

[c]Oncology Institute of Vojvodina, Faculty of Medicine, University of Novi Sad, Sremska Kamenica, Serbia

[d]Institute of Molecular Genetics and Genetic Engineering, University of Belgrade, Belgrade, Serbia

[e]Slovenian NMR Centre, National Institute of Chemistry, Ljubljana, Slovenia

† Electronic supplementary information (ESI) available. See DOI: 10.1039/c6ra03879d

‡ These authors contributed equally to this work.

Published on 14 April 2016. Downloaded by National Library of Serbia on 13/03/2018 11:39:29.

however their significantly better efficacy has not been expressed when it comes to multiple drug resistance.[2] Moreover, studies on the nanoparticle chitosan–DOX have shown reduced efficiency, in *in vitro* tests, compared to DOX applied alone. This phenomenon can be attributed to covalent bonding of DOX to chitosan[17] and consequently DOX's inability to access the cell nucleus. These results indicate the importance of research focused on development of nanocomposites based on noncovalent interactions of DOX and nanocarriers. Different carbon nanocarriers of DOX, such as nanotubes[18] and fullerene conjugates[19] have also been investigated. Fullerenol–DOX conjugate has been shown to suppress proliferation of cancer cell-lines through a G2-M cell cycle. In the *in vivo* murine tumor model, the fullerenol–DOX conjugate exhibited similar antitumor efficacy as DOX, without showing the typical adverse effects of DOX. Liu *et al.* have synthesized fullerene-conjugated DOX and investigated its cytotoxic activity on human breast cancer cells (MCF-7).[20] In comparison to DOX, the fullerenol–doxorubicin conjugate showed better antiangiogenic potential.[19] Fullerenol was tested against sensitive tumor cell lines in a model system of DOX-induced cytotoxicity. It was found that fullerenol applied half an hour before DOX highly decreased DOX-induced cytotoxicity even at nanomolar concentrations.[21] Assessment of nanoparticles efficacy as drug delivery systems should, beside examination of cytotoxicity of nanocomposite itself, also include assessment of their potential to induce DNA damage. Moreover, induction of DNA damage in cancer cells was recognized as therapeutic strategy for killing cancer.[22] Related to this, widely accepted, quite appropriate and highly recommended test for genotoxicity evaluating and screening of nanomaterials is the *in vitro* micronucleus (MN) assay.[23] Taken all the previously mentioned into account, we opted for MN test to analyze the influence of the FNP/DOX nanocomposite on DNA damage and cell proliferation.

Over the last few years, zebrafish were frequently employed for biosafety evaluation of diverse anticancer nanoformulations.[24,25] The production of large number of embryos, rapid early embryonal development, and embryos/larvae transparency make zebrafish a particularly suitable model in toxicological and preclinical studies.[26] Based on the above written, the first aim of our work was to create and characterize a stable nanocomposite composed of the fullerenol nanoparticles and commercial drug DOX. The second aim was directed towards reduction of DOX concentration within the nanocomposite, where the nanocomposite would give better antineoplastic effects on malignant cell lines compared to the commercial drug DOX. Finally, the biosafety evaluation of the novel nanocomposite was investigated on a zebrafish model.

Material and methods

Synthesis of the FNP/DOX nanocomposite

Fullerenol nanoparticles (FNP) are made in a two-step synthesis starting from fullerene C_{60} (purity 99.8%, MER) which was brominated in the presence of a catalyst $FeBr_3$ in order to obtain a symmetric polybrominated derivative $C_{60}Br_{24}$.[27] In the next step, bromine atoms of $C_{60}Br_{24}$ were substituted with hydroxyl groups in alkaline media.[28] Thus obtained polyhydroxylated polyanion C_{60} derivative (FNP) in the form of powder was dissolved in water, and 4 ml of FNP solution concentration 0.111 mM (pH 6.5) was sonicated for 20 minutes at 22 °C. After the FNP solution was sonicated, 0.8 ml of aqueous solution of doxorubicin (Adriablastin®; Pfizer: doxorubicin–hydrochloride 10 mg, lactose 50 mg, methyl-*p*-hydroxybenzoate 1 mg) at concentration 1.84 mM was added. The mixture was stored in dark for 48 h at 22 °C. For the preparation of all solutions, deionized water 17.8 MΩ cm was used.

Dynamic light scattering (DLS) – Zetasizer Nano ZS, Malvern

The hydrodynamic mean diameter of the FNP/DOX nanocomposite was obtained by DLS. All DLS measurements were performed at a wavelength 633 nm with an angle detection of 90°, in aqueous solution at 22 °C. All measurements were done in triplicate.

Nuclear magnetic resonance (^{1}H NMR)

Nuclear magnetic resonance spectra were obtained by Varian Unity Inova 300 MHz with ID/PFG probe and TMSPA as a chemical shift reference substance at $\delta_H = 0.0$ ppm. The effects of different molar ratio of FNP and DOX (nFNP : nDOX = 1 : 13; 4 : 13; 8 : 13) on the chemical shift of the aromatic protons and methyl group of doxorubicin were measured. Chemical shift of methyl group at molar ratio nFNP : nDOX = 1 : 13 was observed one hour after preparation, after a month and after seven days. Chemical shift of aromatic protons in the nanocomposite of molar ratio nFNP : nDOX = 1 : 13 was observed in concentrated sample (1 : 6) as well as in unconcentrated sample.

Atomic force microscopy (AFM)

Morphology and structure of FNP and FNP/DOX in aqueous solution were evaluated using atomic force microscopy (AFM). Surface topography and phase images were simultaneously acquired by standard AFM tapping mode using a commercial SNC (Solid Nitride Cone) AFM probe (NanoScience-Team Nanotec GmbH), with the tip radius lower than 10 nm. Highly orientated pyrolytic graphite (HOPG) was used as a surface. Multimode quadrex SPM with a Nanoscope IIIa controller (Veeco Instruments, Inc.) operated under ambient conditions was used. AFM measurements of FNP and FNP/DOX were done in aqueous solution after 48 h storage in dark at 22 °C. It was also measured FNP/DOX in aqueous solution, after 30 day storage in dark at 22 °C.

Transmission electron microscopy (TEM)

Aqueous solution of FNP was applied to copper grid 300 mesh, dried at room temperature and measured using transmission electron microscopy (TEM): JEM 2010F, STEM unit, BF, DF STEM detector, Oxford instruments ISIS 300 EDXS, Gatan PEELS 677, Gatan off-axis TC camera, Auto-alignment system Jeol Motor driven OA. TEM measurements of FNP were done immediately after sonication as well as after 48 h storage in dark at 22 °C.

 This journal is © The Royal Society of Chemistry 2016

Published on 14 April 2016. Downloaded by National Library of Serbia on 13/03/2018 11:39:29.

Cell lines

Two human breast adenocarcinoma cell lines were used in the study: MCF-7, estrogen receptor-positive (ATCC, HTB22), and MDA-MB-231, estrogen receptor-negative (ATCC, HTB-26). The cells were grown in Dulbecco's modified Eagle's medium (DMEM, PAA) with 4.5% of glucose, supplemented with 10% of fetal calf serum (FCS, PAA) and antibiotics: 100 IU per cm^3 of penicillin and 100 μg cm^{-3} of streptomycin (ICN Galenika). The cells were sub-cultured twice a week and a single cell suspension was obtained using 0.25% trypsin in EDTA (Sigma-Aldrich). All cell lines were cultured in flasks (Costar, 25 cm^2) at 37 °C in the 100% humidity atmosphere and 5% of CO_2. Exponentially growing cells were used throughout the assays. Viability of cells used in the assay was over 95%.

Cell treatment

MCF-7 and MDA-MB-231 cells were plated in culture flasks at density of 1×10^6 per 25 cm^2. Cells were treated with the following three substances: DOX, FNP and FNP/DOX for 2 h, 4 h, 24 h and 48 h. Two concentrations of DOX, 0.1 μM and 0.01 μM were used in the assays. The concentrations of FNP/DOX in the assays were also 0.1 μM and 0.01 μM calculated on DOX, while the concentrations of FNP were 0.111 mM and 0.0111 mM. After the exposure time, the cells were harvested by trypsin/EDTA, washed twice with cold PBS, resuspended in PBS to reach the concentration of 1×10^6 cells per ml, and then used in dye exclusion test, drug uptake assay and cell cycle analysis. All the treatments and following assays were done in triplicate.

Dye exclusion test

The cells treated with FNP, DOX and FNP/DOX, as well as the control untreated cells were harvested at different exposure times (2, 4, 24, and 48 hours of exposure), resuspended in 1 ml of PBS and counted manually in a haemocytometer chamber. Viable cell number was determined by using 0.04% trypan blue and was expressed as a total cell number.

Uptake of DOX and FNP/DOX nanocomposite – flow cytometry analysis

MCF-7 and MDA-MB-231 cells were exposed to 0.1 μM DOX and 0.1 μM FNP/DOX. MCF-7 cells were additionally exposed to 0.01 μM DOX since it was not possible to record the flow cytometry signal for 0.1 μM FNP/DOX due to its high cytotoxicity after a 24 h treatment. After the defined time intervals (2 h, 4 h, 24 h, and 48 h) the cells were harvested by trypsin/EDTA, washed twice with cold PBS, and resuspended in 250 μl of PBS before the measurements. Fluorescence histograms were recorded with the BD FACSCalibur (Beckton Dickinson) flow cytometer and analyzed by the Cell Quest software. Argon ion laser was used; excitation wave length was 488 nm, emission signals were collected between 565 nm and 630 nm. The gate was arbitrary set for the detection of green fluorescence (FCS 1.00 Lin, FL2 476, 1.00 Log). To generate each histogram 15.000 events were acquired per sample. The results are presented as a mean fluorescence in arbitrary units (A.U.).

Cell cycle analysis

Untreated cells and cells treated with FNP, DOX and FNP/DOX, were washed in cold PBS, fixed and incubated for 30 minutes in 70% ethanol on ice, centrifuged, and thereafter incubated with 500 μl of RNase A (100 units per mL, Sigma-Aldrich) and 500 μl propidium iodide (400 μg ml^{-1}, Sigma-Aldrich) for 30 minutes at 37 °C. The cell cycle was analyzed by the FACS Calibur E440 (Becton Dickinson) flow cytometer and the CellQuest software. The results are presented as a percentage of the cell cycle phases.

The cytokinesis-block micronucleus assay (CBMN)

The CBMN assay was performed according to published procedures[29] with some minor modifications related to staining. The MDA-MB-231 and MCF-7 cells were seeded in 6 well plates at a density of 1.5×10^5 cells per well. After 24 h of the cells incubation DOX or FNP/DOX were added in different concentrations.

The following concentrations of DOX and FNP/DOX were used on the MDA-MB-231 cell line: 0.06 μM, 0.03 μM, 0.01 μM and 0.007 μM and on MCF-7 cell line: 0.09 μM, 0.04 μM, 0.02 μM and 0.01 μM. After the 24 h treatment, the medium was replaced with a fresh one and cytochalasin-B was added to the cell cultures at a final concentration of 6 μg mL^{-1}. The incubation continued for the next 24 h. Thereafter, cells were detached by trypsin/EDTA, collected by centrifugation, briefly exposed to a cold hypotonic solution (0.56% KCl) and fixed three times with methanol : glacial acetic acid (3 : 1, v/v). Air-dried slides were stained with 2% Giemsa in distilled water for 9 min. For each concentration, a CBMN assay was performed in triplicate and more than 1000 cells were analyzed. Standard criteria were used for the micronuclei identification.[38] Monitored values included the number of mononucleated, binucleated and multinucleated cells, incidence of micronuclei and proliferative division index (PI). Micronucleus incidence was presented as a number of micronuclei per 1000 examined binuclear cells. PI was calculated according to the formula: $PI = (M_1 + 2M_2 + 3(M_3 + M_4))/N$, where M_1–M_4 represent the numbers of cells with 1–4 nuclei, respectively, and N is the total number of scored cells.[29] The PI is a measure of the average number of cell cycles that a cell population passes through, considering both tri-nucleated and tetra-nucleated cells in the same category.[30]

In vitro data analysis

Data are presented as mean ± SD. The statistical analysis was performed using the legal SPS program version 17. Student's *t*-test was used to compare means in the DET assay, while differences between the control and the exposed groups for *MN* were analyzed by a non-parametric test; Mann–Whitney *U* test and ANOVA. The differences were considered significant when $p < 0.05$ and $p < 0.001$.

Fish embryo toxicity assay

Adult zebrafish (*Danio rerio*, wild type) were obtained from a commercial supplier (Pet Centar, Belgrade, Serbia) and

Published on 14 April 2016. Downloaded by National Library of Serbia on 13/03/2018 11:39:29.

maintained in the fish medium (2 mM $CaCl_2$, 0.5 mM $MgSO_4$, 0.7 mM $NaHCO_3$, 0.07 mM KCl) at 27 ± 1 °C and 14 h light/10 h dark cycle, and regularly fed twice a day with commercially dry flake food supplemented with *Artemia nauplii* (TetraMin™ flakes; Tetra Melle, Germany). Shortly after spawning, eggs were collected, twice rinsed from debris in fresh fish medium and transferred into a Petri dish filled with the fish medium. Prior to use, fish medium was aerated at least for 1 h and pre-warmed to 27 °C.

Eggs at 4 h post fertilization (hpf) were examined under a stereomicroscope (PXS-VI, Optica) for viability and treated with six different concentrations (2.3, 4.6, 9.2, 46, 92 and 920 μM) of tested substances and 0.25% DMSO was used as negative control. Embryos were then individually transferred into 24-well plates containing 1000 μl of test solution, 10 embryos per well, and incubated at 27 °C. Experiments were repeated three times, using 30 embryos per concentration.

Apical endpoints (Table S3†) used for toxicity evaluation were recorded according to OECD (236) guidelines for testing of the chemicals[31] at every 24 h for four consecutive days using an inverted microscope (CKX41; Olympus, Tokyo, Japan). At 96 hpf, the embryos were anesthetized by addition of 0.1% (w/v) tricaine solution (Sigma-Aldrich, St. Louis, MO), photographed and killed by freezing at −20 °C for ≥24 h.

Determination of the LC_{50} value (lethal concentration for 50% embryos) was performed by the program ToxRatPro (ToxRat®, Software for the Statistical Analysis of Biotests, ToxRat Solution GmbH, Alsdorf, Germany, Version 2.10.05) using probit analysis with linear maximum likelihood regression.

All the experiments involving zebrafish were performed in compliance with the European directive 86/609/EEC and the ethical guidelines of The Guide for Care and Use of Laboratory Animals of the Institute of Molecular Genetics and Genetic Engineering, University of Belgrade.

Results and discussion

An anthracycline antibiotic DOX is commonly used in the treatment of a wide spectrum of cancers. The exact antitumor mechanism of DOX still remains unclear. It is known that DOX intercalates into DNA and inhibits topoisomerase II activity preventing DNA replication and cell division.[32–34] DOX organ toxicity, especially cardiotoxicity and multidrug resistance, limits its clinical efficacy. DOX enters the cells by diffusion, and exits the cells by active transport *via* P-glycoprotein.[35,36] In new drug formulations DOX is loaded onto various carriers, which enable sustained DOX release in its active form inside the cells, thus ensuring effective DOX concentrations for a longer period of time.[19,37,38] In our previous research we confirmed that fullerenol strongly inhibits DOX-induced cytotoxicity in human malignant cell lines,[21] as well as its cardio and hepatoprotective effects in *in vivo* experiments on healthy and malignant rat models.[39,40] In this research we have used chemical properties of polyanion nanomolecule fullerenol for the formation of the stable nanocomposite with DOX from the commercial drug Adriablastin®.

Physico-chemical and nanocharacterisation of FNP/DOX nanocomposite

^{1}H NMR spectra of different molar ratios *n*FNP : *n*DOX (8 : 13; 4 : 13 and 1 : 13) were recorded in order to investigate intermolecular interactions between fullerenol and DOX in the FNP/DOX nanocomposite. The increase in molar ratio of FNP leads to reduction and loss of signals assigned as aromatic protons at δ 7.76 ppm (t), 7.64 ppm (d), 7.48 ppm (d), and the signal at δ 1.32 ppm (d) assigned as methyl group of DOX sugar component (ESI Fig. S1†). Furthermore, chemical shift of DOX methyl group in molar ratio 1 : 13 was obtained as well (ESI Fig. S2†). There was a significant difference in the position and shape of the signals of methyl group of sugar component of DOX over time. After preparation, spectrum changes and a new doublet appears at δ 1.32 ppm. After seven days, a triplet-like shape signal appears at δ 1.18 ppm, and one month after the preparation becomes the predominant signal. The other family of studied signals was in the region of aromatic protons of DOX, whose chemical shifts are depicted (ESI Fig. S3†). Increase in concentration of the same molar ratio 1 : 13 led to a shift towards higher magnetic field and disappearance of the middle doublet at δ 7.76 ppm.

Molecular interactions between DOX and FNP are observed through changes in the chemical environment of aromatic and methyl groups. Observed changes in spectra are for the signals of aromatic and methyl group in the sugar part of DOX molecule. The ^{1}H NMR data clearly show that anthracycline protons and methyl group in sugar ring moieties are involved in forming of the FNP/DOX nanocomposite. On the basis of ^{1}H NMR measurements it can be concluded that after a longer period of time molecular interactions between FNP and DOX become more pronounced. We performed diffusion type experiments on FNP and DOX sample with the ratio 1 : 13. A significant change in size of the free molecule of DOX and expected assembly of DOX interacted to FNP in the FNP/DOX nanocomposite cannot be inferred on the basis of relatively similar diffusion coefficients ($\sim 2.5 \times 10^{-6}$ cm^2 s^{-1}). Similar diffusion coefficient of DOX and FNP/DOX in molar ratio *n*FNP : *n*DOX = 1 : 13 indicates a slow process of intermolecular interactions in the formation of the FNP/DOX nanocomposite.

By comparing the FTIR results of the nanocomposite and components (FNP and DOX), no differences in spectra were observed (results are not presented).

In Fig. 1 we can see the distribution of the number of FNP in water (17–42 nm, max 24 nm, 35%) and the FNP/DOX nanoparticles ranging from 25 to 67 nm, the most prevailing are the 38 nm particles (31%). From these results it can be noticed that DOX in FNP/DOX did not significantly affect the size of the composite compared to FNP. Further, zeta potential measurements have shown that FNP in aqueous solution was −20 mV charged while the FNP/DOX nanocomposite was −6 mV charged (ESI Fig. S4†).

Nanocharacterisation of FNP and FNP/DOX nanocomposite was done by using AFM. Samples were recorded after being stored in dark at 22 °C for 48 h and after a month period.

 This journal is © The Royal Society of Chemistry 2016

Published on 14 April 2016. Downloaded by National Library of Serbia on 13/03/2018 11:39:29.

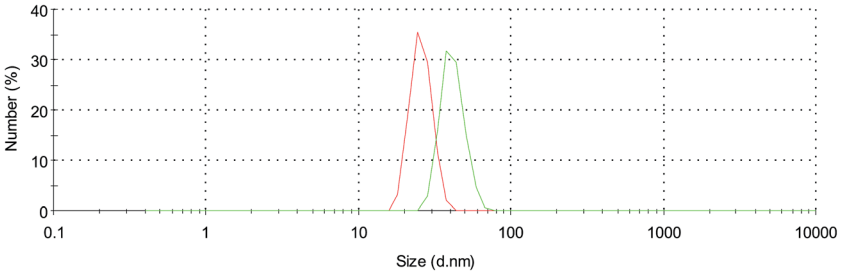

Fig. 1 Distribution by number of FNP and FNP/DOX nanocomposite particles after the 48 h exposure to 22 °C. Red line refers to FNP and green refers to FNP/DOX. Three independent measurements were performed and one representative is displayed. Measurements were done by Zetasizer Nano based on method of dynamic light scattering.

On Fig. 2 are presented the AFM measurements of the FNP aqueous solution at pH = 6.5, which seems to be an inhomogeneous sample (Fig. 2A). The presence of nanoparticles is evident, one of which is of 79 nm and consists of two particles (Fig. 2B), a smaller one of 29 nm and a bigger one of 50 nm, both with the height of 5.1 nm, which is confirmed by the corresponding cross-section (Fig. 2C). These results are comparable with the results published by Assemi *et al.*[41] Bigger particles in the FNP sample consist of 2–4 particles of 30 nm, however the presence of particles bigger than 150 nm was not detected. The fullerenol nanoparticles are distributed on HOPG terraces, which indicates their polarity and is in accordance with the zeta potential measurements and studies data.[42] Fig. 2D presents 3D morphology of fullerenol nanoparticles on HOPG, where the structure of bigger particles can be clearly seen.

Fig. 3 presents the AFM results of the FNP/DOX nanocomposite after 48 h storage in dark at 22 °C. By comparing the measurements of FNP (Fig. 2) and the nanocomposite (Fig. 3)

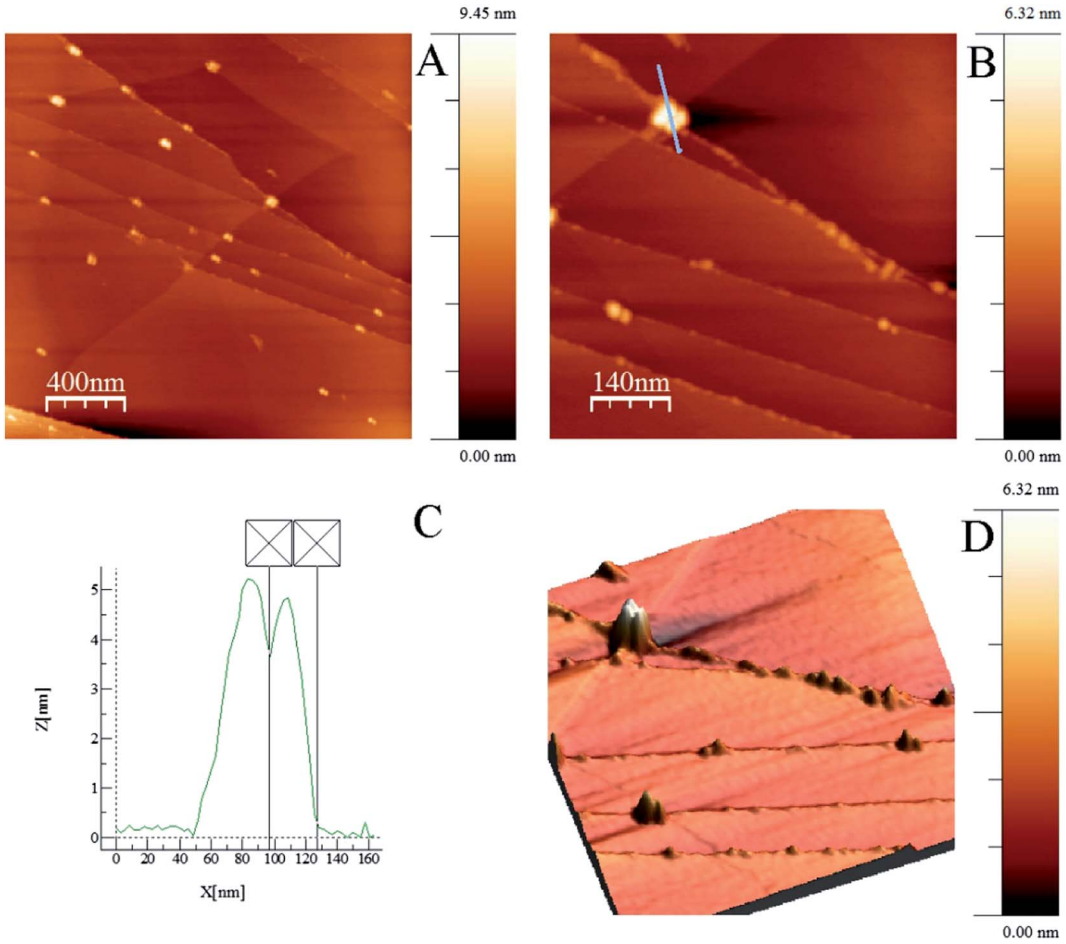

Fig. 2 AFM measurement of FNP aqueous solution on HOPG surface, after 48 h storage in dark at 22 °C; (A) scale 2000 × 2000 nm^2 (B) scale 710 × 710 nm^2 (C) corresponding cross-section (D) 3D image.

Published on 14 April 2016. Downloaded by National Library of Serbia on 13/03/2018 11:39:29.

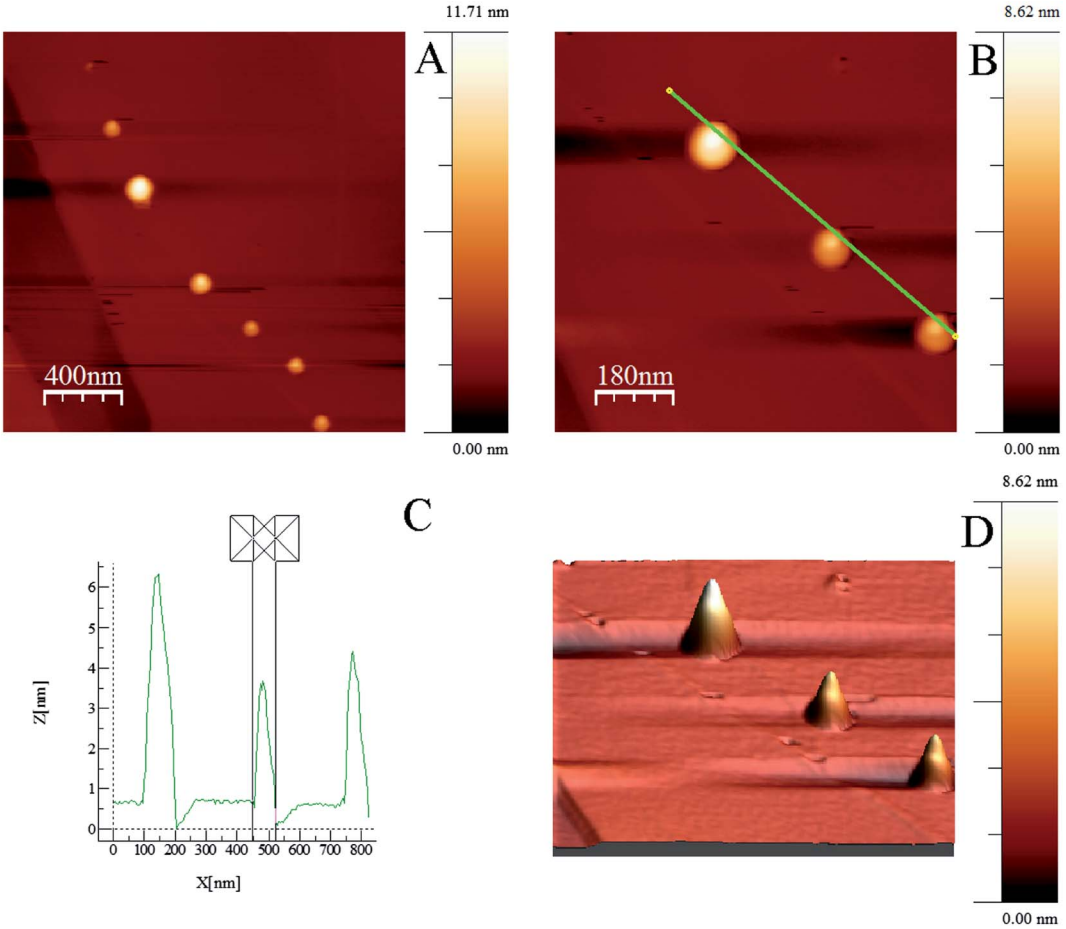

Fig. 3 AFM measurement of the FNP/DOX nanocomposite on HOPG surface, after 48 h storage in dark at 22 °C; (A) scale 2000 × 2000 nm^2 (B) scale 670 × 670 nm^2 (C) corresponding cross-section (D) 3D image.

significant changes in morphology can be observed. The FNP/DOX nanocomposite particles (Fig. 3A and B) are of 37.5 nm, 39.2 nm and 86 nm and unlike the FNP particles (Fig. 2A and B), do not seem to be formed of several smaller particles. The nanocomposite particles are distributed over the HOPG terraces, which indicate their polarity. Fig. 3C shows corresponding cross-section of the FNP/DOX nanocomposite particles with the height ranging from 2.5 nm to 6 nm, whereas Fig. 3D depicts a 3D morphology of the nanocomposite. By comparing the 3D figures of FNP (Fig. 2D) and the FNP/DOX nanocomposite (Fig. 3D) the obvious difference in surface morphology can be noticed.

AFM measurement of the FNP/DOX nanocomposite after a 30 day storage in dark at 22 °C is presented in ESI Fig. S5.† The morphology analysis shows the presence of dominant nanoparticles of 30–40 nm, as well as the presence of crossed nanonicles of micron length made of nanoparticles of 40 nm and with the thread width ranging from 30–40 nm, which is confirmed by the corresponding cross-section (ESI Fig. S5b and c†). 3D morphology of FNP/DOX nanocomposite at HOPG can be seen in ESI Fig. S5d.† It can be concluded that present particles, which do not form nanothreads, are quite similar in morphology to those that were measured after 48 h. Comparison of AFM results for two different ages of FNP/DOX nanocomposite leads to conclusion that with time particles of 30–40 nm self-assemble into stable nanothreads of micrometer scale. Our assumption is that nanoparticles in a nanothread are mutually attracted by polar interactions.

TEM measurements of FNP aqueous solution after sonication and 48 h storage in dark at 22 °C is depicted on Fig. 4. Fullerenol nanoparticles of 2 nm (yellow arrow) are made of 2–3 fullerenol molecules. The presence of stable FNP aggregates of approx. 20 nm (red arrow) is evident, as well as the one of the particles ranging from 30–60 nm (blue arrow) that are formed of numerous smaller stable aggregates of 2 nm. After sonication of fullerenol aqueous solution, only particles of 2 nm were present (ESI Fig. S6†).

Changed morphology of FNP/DOX particles in comparison to FNP particles most probably suggests the changes in FNP structure in the presence of DOX. It is possible that during the formation of a stable FNP/DOX nanocomposite DOX molecules stay trapped inside the nanoparticle (Fig. 5).

The size, charge, structure and morphology of drug carriers are of great importance in biological applications because these features can affect their biological response as well as drug metabolism.[43,44] If nanoparticles are larger than 300 nm they can trigger the complement system and be removed from the blood[45] and/or cause thrombosis.[46] For these reasons we

 This journal is © The Royal Society of Chemistry 2016

Published on 14 April 2016. Downloaded by National Library of Serbia on 13/03/2018 11:39:29.

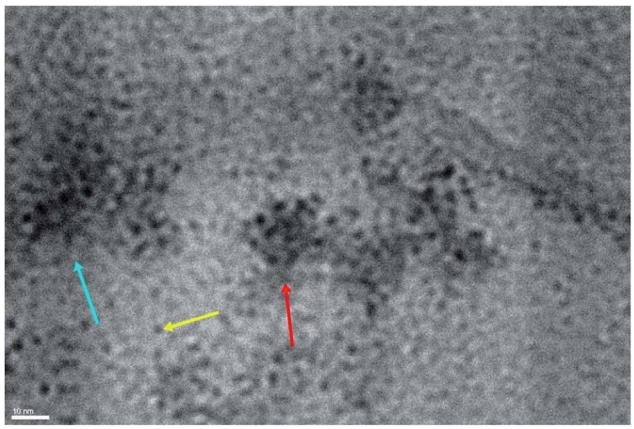

Fig. 4 TEM micrography of fullerenol nanoparticles aqueous solution after sonication and 48 h storage in dark at 22 °C. FNP of 2 nm (yellow arrow), 20 nm (red arrow) and 30–60 nm (blue arrow). Measurements were performed on copper grid 300 mesh.

focused our research on developing stable small-sized FNP/DOX nanocarrier.

The nanocomposite increased cytotoxicity

In this section we would like to point out the reason for using nanomolar concentrations of DOX and FNP/DOX in cell treatments. The plasma kinetics of DOX exhibits an initial half-life of approximately 8 min followed by a terminal half-life of about 30 h.[47] The major exposure to organs occurs during the terminal phase where DOX concentrations are generally less than 0.1 μM.

Cells were exposed to FNP (0.111 mM), DOX and FNP/DOX (0.1 μM and 0.01 μM DOX) for 2 h, 4 h, 24 h, and 48 h and cell number was counted at specified time points (Fig. 6). Free DOX decreased the number of MCF-7 and MDA-MB-231 cells in time-dependent manner up to 24 h. However, cell number was increased after 48 h of treatment in both cell lines. A possible explanation for the increased cell number could be the DOX concentration decrease due to at least two facts: a half-life of DOX that is around 30 hours and DOX easily exits cells by active transport.[34,35]

Furthermore, fluorescence intensity of free DOX in both cell types was also decreased at the same time point (Fig. 7). The FNP/DOX nanocomposite, compared to free DOX, at equivalent DOX concentration (0.1 μM) significantly ($p < 0.05$) decreased MCF-7 cell number after a 4 h treatment. MCF-7 cell number decreases by time exposure, reaching the minimum value after 48 h of incubation. Ten-fold smaller concentration of FNP/DOX also decreased the MCF-7 cell number after a longer incubation period, being more effective at a 48 h treatment (Fig. 6). These results are in accordance with fluorescence intensity of FNP/DOX (Fig. 7). Compared to the MCF-7 cells, the MDA-MB-231 cells were found less sensitive to both free DOX and FNP/DOX. The similar number of FNP-treated and untreated cells confirms that FNP did not impair cell viability up to 4 hours, while the decreased cell number was found after 24 h and 48 h treatment ranged from 12% to 15%, compared to untreated

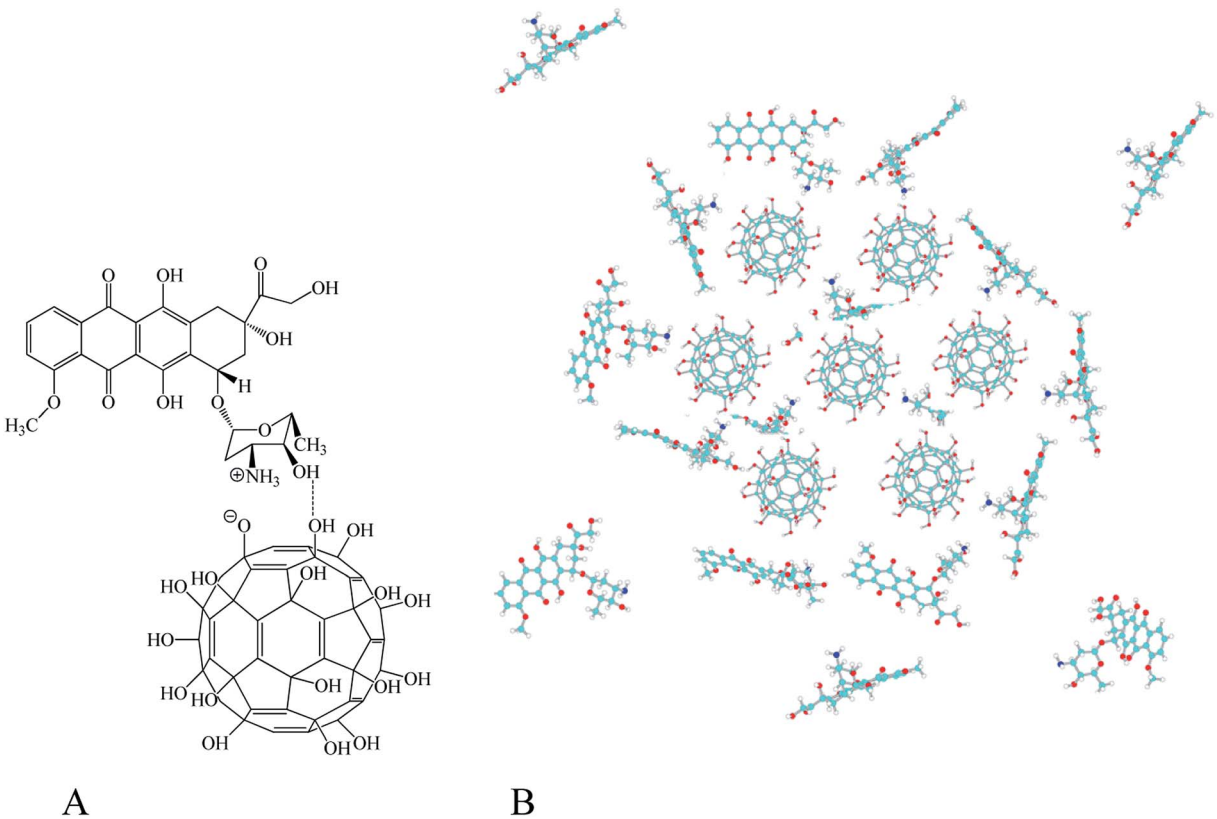

Fig. 5 (A) Polar interaction between fullerenol and DOX. (B) Hypothetical preview of FNP/DOX nanocomposite.

Published on 14 April 2016. Downloaded by National Library of Serbia on 13/03/2018 11:39:29.

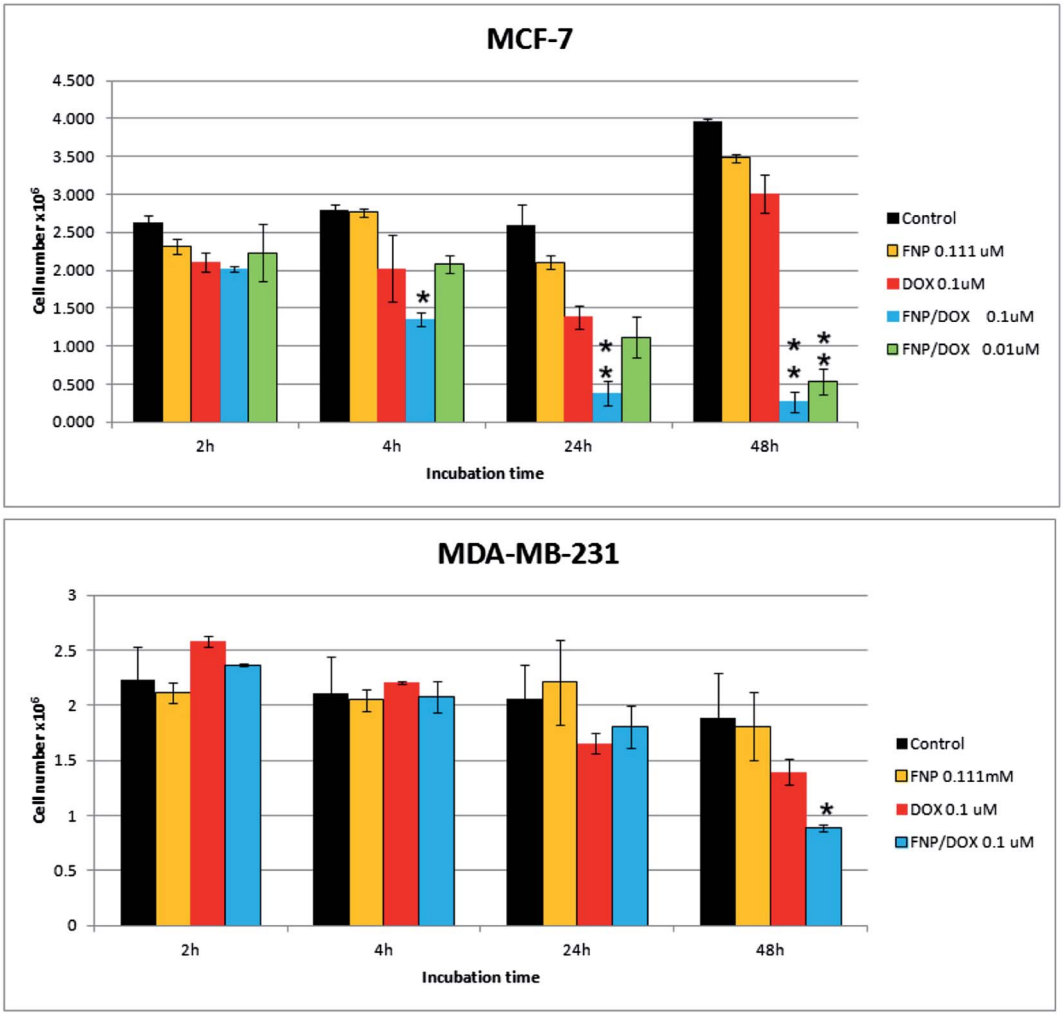

Fig. 6 Cytotoxic effects of DOX and FNP/DOX on human breast cancer cells (MCF-7, ER^+; MDA-MB-231, ER^-) performed by dye exclusion assay as a function of time. Data are the results of three independent experiments and are expressed as the mean ± SD. Student's *t*-test was used to compare means.*$p < 0.05$, **$p < 0.01$ compared to the DOX-treated sample.

MCF-7 and MDA-MB-231 cells which is in accordance with the published results.[21]

Interaction of nanostructures with cells depends on nanostructures' size, shape, charge and material properties, but complete understanding of these interactions remain poorly understood.[48–50] Nanoparticles within the 2–100 nm size range alter signaling processes essential for basic cell functions, but 40 nm and 50 nm nanoparticles demonstrated the greatest effects.[49] Intracellular delivery of various DOX-loaded nanoparticles usually resulted in higher cytotoxicity compared to free DOX. The extent of cytotoxic effect depends on size, time and surface modification, as well as on the particle concentration.[51–53] Free DOX was found in cytoplasm and in nucleus of cells, while DOX-loaded nanoparticles were only found in the cytoplasm.[52,53]

Increased cell uptake of DOX *via* the nanocomposite

Internalization of free DOX and FNP/DOX in MCF-7 and MDA-MB-231 cells was analysed by the flow cytometry. A total of 15.000 events were analyzed per sample. MCF-7 and MDA-MB-231 cells were exposed to DOX and FNP/DOX nanocomposite for 2 h, 4 h, 24 h and 48 h at the equivalent DOX concentrations (0.1 μM and 0.01 μM) and DOX fluorescence in the MCF-7 and MDA-MB-231 cells was recorded at specified time points (Fig. 7; ESI Fig. S7†).

Untreated cells were used as a negative control. Fig. 7 and ESI Fig. S7† show that DOX was successfully internalized in the cells, whereas cellular uptake of FNP/DOX was several fold higher (2-fold to 3.7-fold) in both cell types when compared to free DOX.

According to mean fluorescence intensity, uptake of both compounds was better in MCF-7 cells at each time point especially for 2 h and 4 h treatment, although uptake ratio (FNP/DOX *vs.* DOX) was higher in MDA-MB-231 (1.8–2.9 for MCF-7 and 2.6–3.7 for MDA-MB-231). Maximum fluorescence of DOX and FNP/DOX in MCF-7 was observed after 24 hours of incubation. High mean fluorescent intensity of DOX and FNP/DOX in the MCF-7 cells was in accordance with their high sensitivity to effects both, free and DOX-loaded FNP. The number of

 This journal is © The Royal Society of Chemistry 2016

Published on 14 April 2016. Downloaded by National Library of Serbia on 13/03/2018 11:39:29.

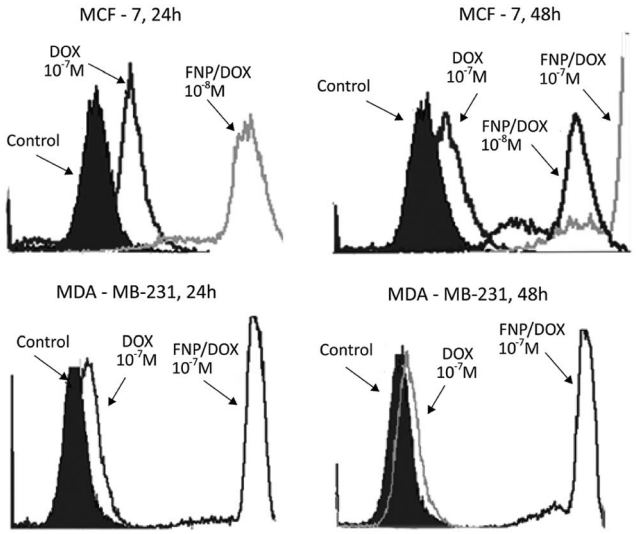

Fig. 7 Uptake of DOX and FNP/DOX by human breast cancer cells (MCF-7, ER^+; MDA-MB-231, ER^-). Control cells and cells treated with DOX and FNP/DOX were incubated at 37 °C for 24 and 48 hours. Fluorescent data were achieved using flow cytometry analysis. Results are presented as overlaid histograms of one representative experiment from three independent experiments with similar results.

the viable MCF-7 cells was significantly decreased ($p < 0.01$) after a 24 hour treatment with 0.1 μM DOX and FNP/DOX (Fig. 6). Since it was not possible to record histogram for FNP/DOX after 24 h at a defined gate setting (FCS 1.00 Lin, FL2 476, 1.00 Log), we treated theMCF-7 cells with 10-fold (one log) smaller FNP/DOX concentration and found that the fluorescence intensity of FNP/DOX was still high and reached maximum value at 24 h (Fig. 7 and ESI Fig. S7†). The fluorescence intensity of DOX and FNP/DOX decreased after 48 hours which is in agreement with the MCF-7 viable cell number. In MDA-MB-231 cell line, maximum uptake of FNP/DOX was achieved after 48 hour of cell treatment. Differences in internalization and cellular uptake behavior of free DOX and various DOX-loaded nanoparticles have previously been observed.[52–54] Generally, uptake of DOX-loaded nanoparticles was successful in several cell types.[52–54] Nanoparticles containing DOX were taken up by cells *via* endocytosis and accumulated in cytoplasm, while free DOX was observed in both cytoplasm and nucleus of the cells showing bimodal life-time distribution.[52] Our results of flow cytometry indicated that FNP/DOX could remarkably increase the uptake of DOX in MCF-7 and MDA-MB-231 cells suggesting that FNP might be a promising intracellular targeting carrier for efficient delivery of antitumor drugs into tumor cells.

The nanocomposite did not affect cell cycle distribution

The cells progress through the series of events (cell cycle) thus leading to cell division and duplication. Flow cytometry enables us to distinguish four distinct phases of the cell cycle: G1 phase, S phase (synthesis), G2 phase (interphase) and M phase (mitosis). The progress of the cell cycle is tightly monitored and regulated and cycling cells are targets in cancer therapy. We studied effects of free DOX and FNP/DOX nanocomposite on the cell cycle perturbations by total DNA staining with propidium iodide. In two independent experiments we found that free DOX arrested MCF-7 cells in G2M phase (Fig. 8).

Our results are in accordance with results of Park *et al.* and Lüpertz *et al.*, who found that DOX in various cells increased cells in G2/M phases.[55,56] Rusetskaya *et al.*, however, found that DOX in the sensitive MCF-7 cells arrested cells in G0/G1 phase of cell cycle.[57]

We found that FNP alone decreased the G2M phase of the MCF-7 cells after 24 h, but increased S phase after 48 h in comparison to control and the DOX-treated cells. The FNP/DOX nanocomposite at both concentrations affected the cell cycle distribution in similar manner by increasing the cell number in S phase of the cell cycle with respect to the G0/G1 cell cycle phase (ESI Table S1†). FNP/DOX also induced an increase in the MCF-7 cells in the sub G1 phase. DOX and FNP/DOX did not significantly affect cell cycle distribution of MDA-MB-231 cells (Fig. 9 and ESI Table S2†).

It is generally accepted that the size and structure of nanoparticles can influence how cell internalizes nanoparticles.[48] In the extensive study of the nanoparticle uptake by cells on cell cycle phases, Kim *et al.* showed that cells in different phases of the cell cycle internalize nanoparticles at similar rates, but after 24 h the concentration of nanoparticles in the cells could be ranked, according to the different phases as: G2/M > S > G0/G1.[58] The same ranking was observed regardless nanoparticle concentration, size or coating material, and regardless cell doubling time and culture media. Our results are partly in accordance with the results of Kim *et al.* who found that nanoparticle uptake had no influence on cell cycle distribution.[58]

The nanocomposite decreased cell proliferation by increasing DNA damages

In this work, we analyzed incidence of micronuclei that reflects a measure of DNA damage. Besides, proliferation index was also determined and it shows the influence of tested substances on cell kinetics. In the assessment of nanocomposite efficacy as drug delivery systems, very important place takes the non-toxicity of nanoparticles used in the antineoplastic delivery. Our previous studies that included micronuclei and chromosome aberrations tests proved that fullerenol within concentration range 5.54–221.6 μM did not show genotoxicity against human peripheral blood lymphocytes and CHO cell lines.[59,60]

In this work, in order to determine genotoxicity of the FNP/DOX nanocomposite, as well as DOX itself, we applied subtoxic concentrations that were previously defined in a serial of experiments conducted according to the scheme for micronuclei assay (data not included).

FNP/DOX and DOX effects on micronuclei incidence of MDA-MB-231 and MCF-7 cell lines after a 24 h treatment are presented in Fig. 10.

Compared to control, DOX depending on concentration increased micronuclei incidence in cell lines MDA-MB-231 and MCF-7 (Fig. 10.), while the cell proliferation was decreased

Published on 14 April 2016. Downloaded by National Library of Serbia on 13/03/2018 11:39:29.

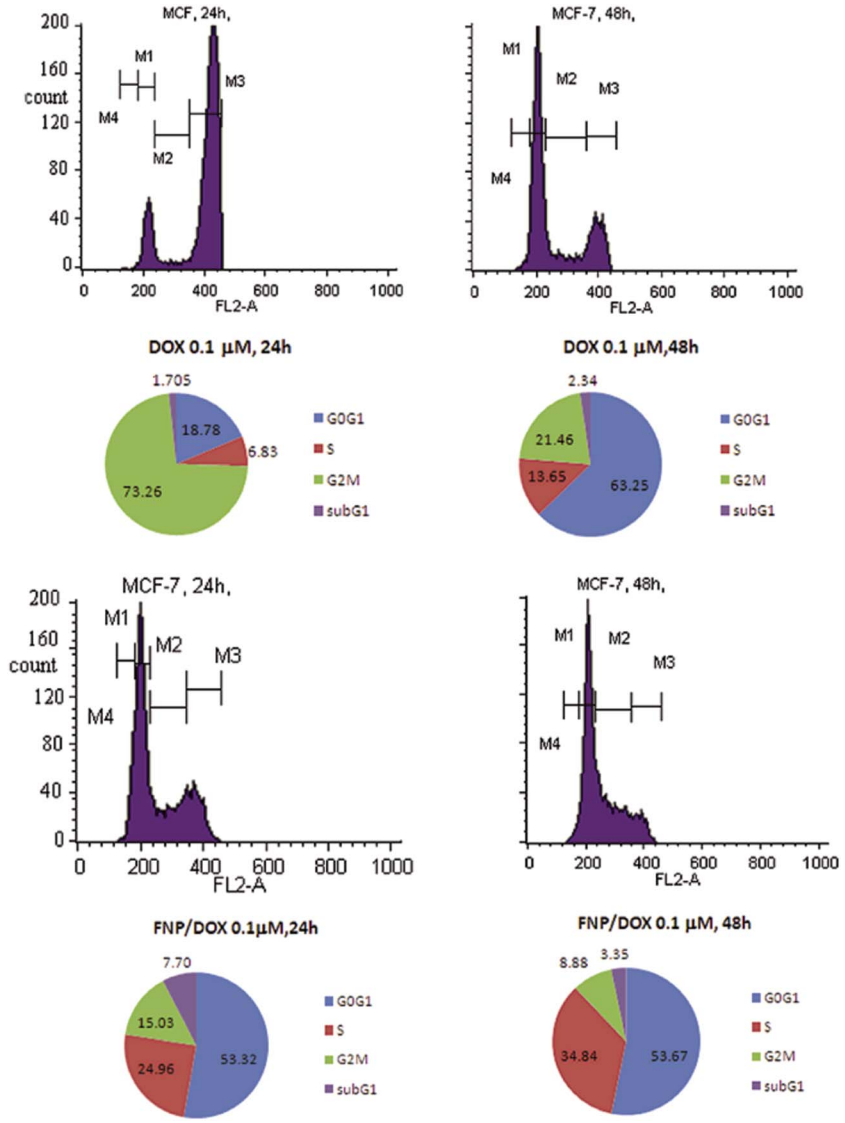

Fig. 8 Distribution of MCF-7 cells between the cell cycle phases (%) in samples treated with DOX and FNP/DOX at 24 and 48 hours. For a clearer review of the cell cycle distribution under each histogram is displayed corresponding graphical pie. Fluorescent data were achieved using flow cytometry analysis. Results present one representative experiment from three independent experiments with similar results.

(Fig. 11). On MDA-MB-231 cell line, FNP/DOX nanocomposite at lower concentrations (0.007 μM and 0.01 μM) induced higher micronuclei incidence in comparison to corresponding concentrations of DOX, while cell proliferation index was significantly lower ($p < 0.05$; $p < 0.001$).

With the increase in FNP/DOX concentration (0.03 μM and 0.06 μM), micronucleus incidence was significantly lower when compared to DOX, however cell proliferation index values also significantly declined. The greatest efficacy of FNP/DOX in comparison to DOX alone on MDA-MB-231 cell line was at concentration 0.01 μM (MN: $p < 0.001$; 654.86: 404.81 and PI: $p < 0.001$; 1.33: 1.47).

On the MCF-7 cell line, with the increase in the FNP/DOX nanocomposite concentration micronucleus incidence increased as well (Fig. 10), whereas proliferation index values were lower in comparison to DOX (Fig. 11).

When compared to 0.02 μM concentration of DOX, 0.02 μM FNP/DOX concentration caused significantly lower micronucleus incidence ($p < 0.05$; 427.45: 349.25) and significantly higher proliferation index ($p < 0.001$; 1.3: 1.39).

Comparing the FNP/DOX nanocomposite effects on different cell lines it can be noticed that at higher concentrations of nanocomposite DNA damage was more expressed in the MCF-7 cell line, unlike in the MDA-MB-231 cell line where more DNA damage occurred at lower concentrations of nanocomposite. Compared to DOX, decrease in cell proliferation index of the MCF-7 cells was more significant at lower nanocomposite concentrations, while in case of MDA-MB-231 a decrease in proliferative index was noticeable at all examined concentrations of nanocomposite.

Different sensitivity of cell lines to FNP/DOX influence is in agreement with results of in the work of Chaudhuri *et al.*, who

 This journal is © The Royal Society of Chemistry 2016

Published on 14 April 2016. Downloaded by National Library of Serbia on 13/03/2018 11:39:29.

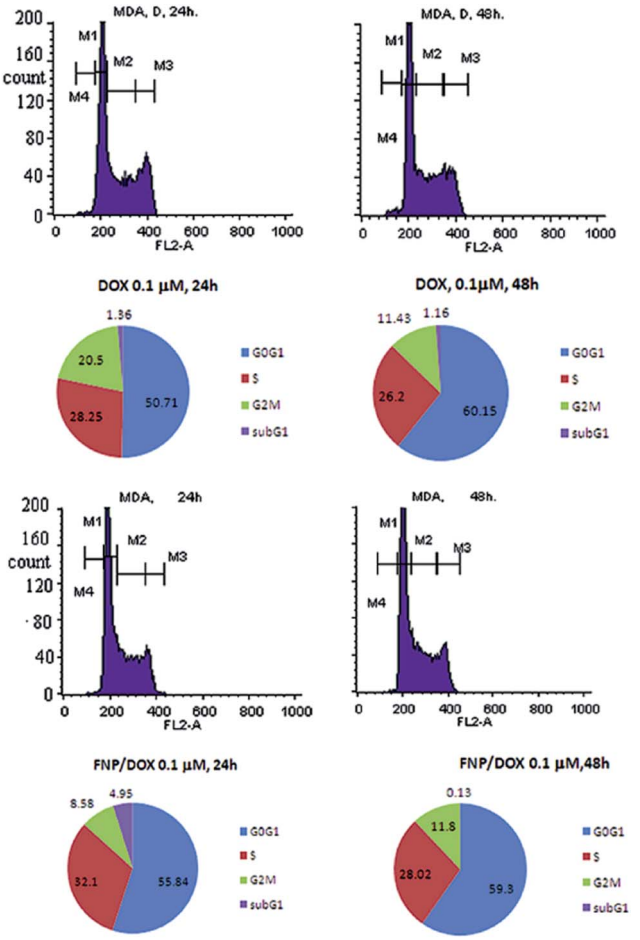

Fig. 9 Distribution of MDA-MB-231 cells between the cell cycle phases (%) in samples treated with DOX and FNP/DOX at 24 and 48 hours. For a clearer review of the cell cycle distribution under each histogram is displayed corresponding graphical pie. Fluorescent data were achieved using flow cytometry analysis. Results present one representative experiment from three independent experiments with similar results.

also claimed that conjugated fullerenol $C_{60}(OH)_{16-24}$ and doxorubicin suppressed the proliferation of cancer cell lines, but with less efficiency against human breast cancer cell line MDA-MB-231 than mouse melanoma and lung carcinoma cell line.[19] The authors explained this with different susceptibility of MDA-MB-231 and the mouse cancer cells to the internalization of the FNP/DOX into the cells and into the lysosomes. Our results are in a complete agreement with this, showing that the FNP/DOX nanocomposite at subcytotoxic concentration decreased breast cancer cell line proliferation more than free DOX, and even caused DNA damage.

The nanocomposite reduced toxicity on zebrafish embryos

In this study, the zebrafish model was used to evaluate *in vivo* toxicity of the nanocomposite FNP/DOX in comparison to DOX and FNP alone, by assessing lethality, morphological abnormalities and cardiac functions of treated embryos. In the 4 day assay, the tested compounds exhibited different toxic effects in dose- and time-dependent manner (Fig. 12A). At the highest tested compound concentration of 960 µM, FNP and FNP/DOX precipitated from the zebrafish medium, therefore this concentration was not taken into consideration. In the range of FNP concentrations up to 96 µM, involving those at which FNP was present in the highest tested dose of nanocomposite, FNP did not show any adverse effects on the survival or the development of zebrafish embryos (ESI Table S2†), suggesting that FNP present in each tested nanocomposite dose should not be toxic. An exception was a concentration of 96 µM FNP, where only 11% of embryos was affected (Fig. 12B).

Under the DOX and FNP/DOX treatments, the mortality rate of the zebrafish embryos increased in dose-dependent manner (Fig. 12A), whereas the significant difference in the overall toxicity between these treatments has been detected (Fig. 12B). At doses ≤4.6 µM, neither DOX nor FNP/DOX showed any signs of toxicity on zebrafish embryos (data not shown), while already at concentration of 9.2 µM DOX was significantly more toxic than FNP/DOX ($P = 0.002$, χ^2 test; $n = 90$; Fig. 12B), as evaluated from the score of lethal and teratogenic effects. As shown in Fig. 12, the survival rate of embryos treated with 92 µM or 46 µM of FNP/DOX was significantly higher than under the same doses of DOX ($P < 0.001$, χ^2 test; Fig. 12B). The obtained LC_{50} values of 115.86 µM for FNP/DOX and 46.25 µM for DOX indicated that survival rate of zebrafish embryos upon nanocomposite treatment was 2.5 times higher than upon the DOX treatment. Thus the fullerenol-based nanosystem for DOX loading significantly reduced DOX lethality in the zebrafish model. The statistical analysis also confirmed a significantly lower toxicity of FNP/DOX in comparison to DOX alone, at concentrations of 92 µM or 46 µM ($P < 0.0001$, χ^2 test; Fig. 12B).

Besides the significant differences in lethal outcome, different time-dependent and dose-dependent teratogenic responses have been observed in the zebrafish embryos upon the FNP/DOX and DOX treatments (ESI Tables S3 and S4†), particularly at cardiovascular level. While DOX was disturbing cardiovascular functions already at 48 hpf at doses ≥9.2 µM, with most embryos developing pericardial edemas upon 92 µM and 46 µM of DOX, the cardiotoxicity caused by the nanocomposite on this early developmental stage was detected only at 92 µM (ESI Tables S3 and S4†). Cardiotoxicity of nanocomposite was evident at 72 hpf at 46 µM concentration (Fig. 13A). Importantly, pericardial edemas in zebrafish embryos developed up to 96 hpf were significantly smaller comparing the 92 µM nanocomposite with 46 µM DOX (Fig. 13B). Furthermore, when exposed to 46 µM FNP/DOX, a total of 13% of embryos did not develop pericardial edema nor any other cardiovascular defects even at 96 hpf, whereas all the DOX-treated ones suffered cardiovascular defects, including edemas, already at 48 hpf.

Earlier and higher cardiotoxicity in DOX-treated groups than in FNP/DOX treated groups of embryos has also been observed through a significantly slower heart beating rate (Fig. 14) and impaired caudal and yolk sac circulation, that resulted in slower growth and faster lethal outcome of

Published on 14 April 2016. Downloaded by National Library of Serbia on 13/03/2018 11:39:29.

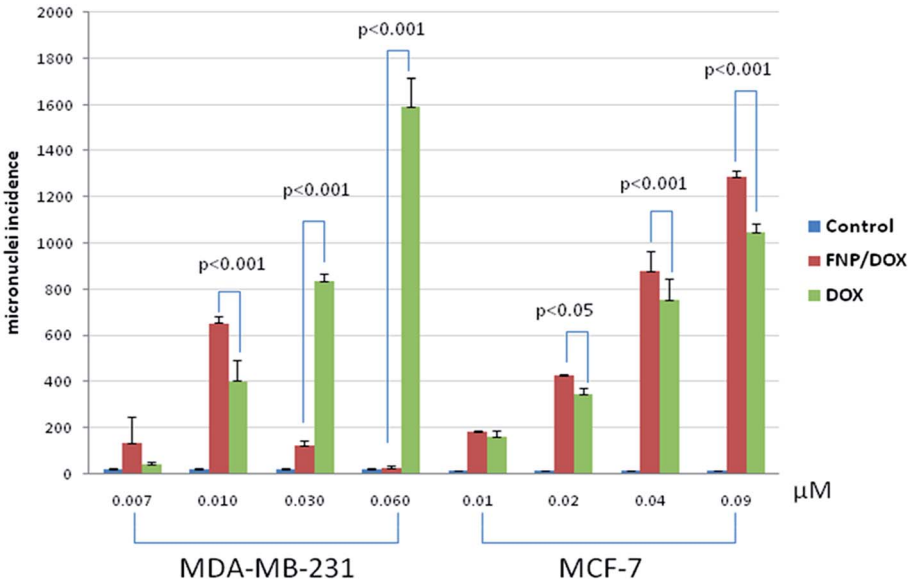

Fig. 10 FNP/DOX and DOX effects on micronuclei incidence of the MCF-7 and MDA-MB-231 cell lines after a 24 h treatment. Results are presented as the mean ± SD of one representative experiment from three independent experiments with similar results. Mann–Whitney *U* test and ANOVA were used to evaluate differences between the groups. The differences were considered significant when $p < 0.05$ and $p < 0.001$.

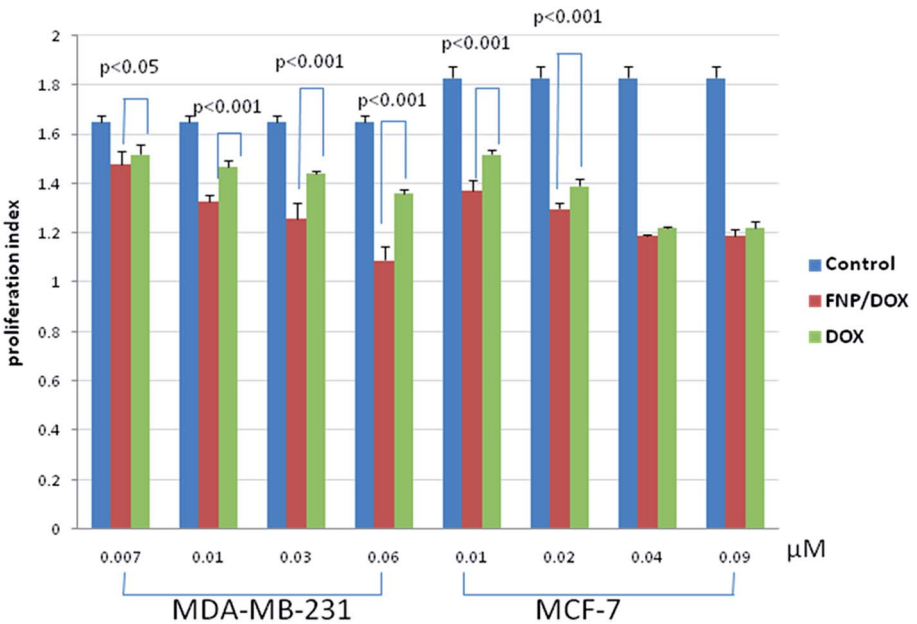

Fig. 11 FNP/DOX and DOX effects on proliferative index of MCF-7 and MDA-MB-231 cell lines after 24 h treatment. Results are presented as the mean ± SD of one representative experiment from three independent experiments with similar results. Mann–Whitney *U* test and ANOVA were used to evaluate differences between the groups. The differences were considered significant when $p < 0.05$ and $p < 0.001$.

embryos under the DOX regime. Both compounds, applied in doses of 92 μM and 46 μM, reduced the embryo heart beating rate after 96 h exposure, whereas FNP/DOX decreased cardiac rhythm at a significantly lesser extent than DOX ($P < 0.0001$, χ^2 test; Fig. 14). At concentration of 92 μM, DOX prevented caudal circulation of all the embryos and caused accumulation of red blood cells (RBC) in the pericardial sac, probably due to a very weak heart contractility without RBC pass through it, while body circulation was barely observed upon 46 μM DOX. On the other hand, a higher rate of heart contractions and blood circulation through heart and caudal vessels were easily observed in most embryos under 46 μM FNP/DOX after the 96 h treatment and, at lesser number of embryos under 92 μM FNP/DOX.

Along with prominent cardiovascular defects, treated zebrafish embryos also showed some dose-dependent skeletal

 This journal is © The Royal Society of Chemistry 2016

Published on 14 April 2016. Downloaded by National Library of Serbia on 13/03/2018 11:39:29.

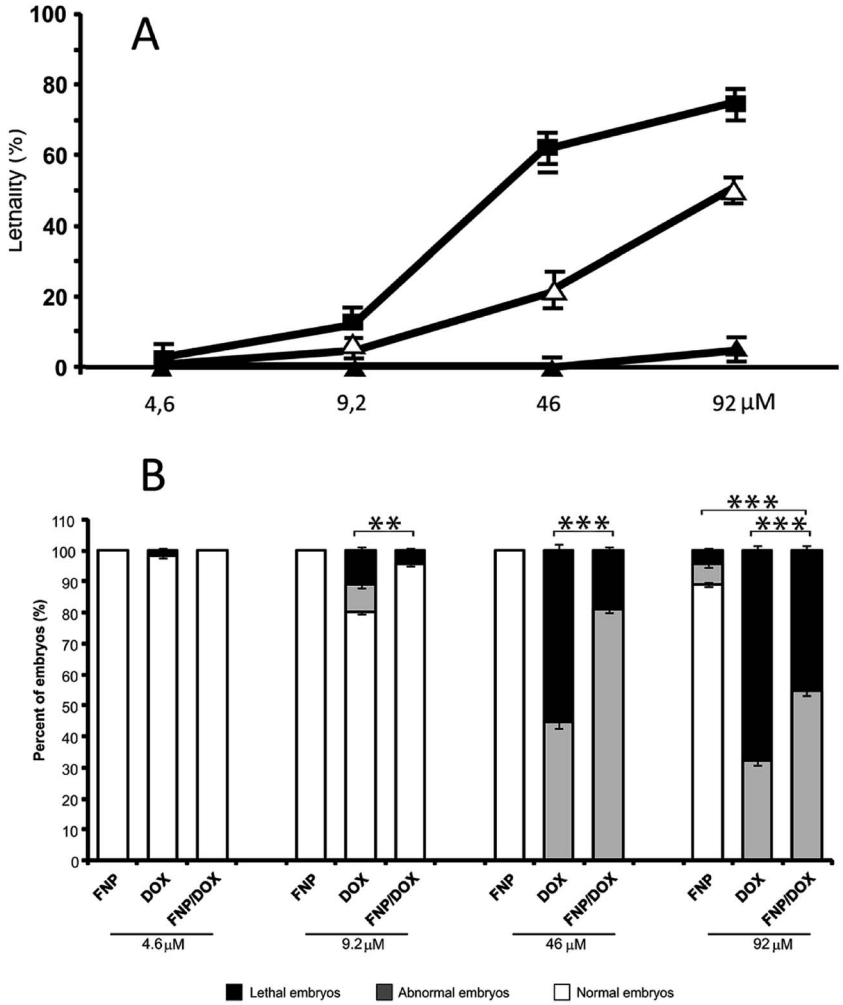

Fig. 12 Dose-responsive curve of zebrafish embryos lethality at 96 hours post fertilization (hpf) under different doses of fullerenol (FNP), doxorubicin (DOX) and nanocomposite (FNP/DOX) (A). Toxic effects (mortality and teratogenicity) induced in zebrafish embryos by fullerenol (FNP), doxorubicin (DOX) and nanocomposite (FNP/DOX) exposure at 96 hpf (B). Statistically significant differences in total toxicity (sum of dead and abnormal embryos) between the tested compounds are denoted by $*P < 0.05$, $**P < 0.01$, $***P < 0.001$.

deformities, which were more obvious in DOX-treated groups of embryos. Under doses of DOX and FNP/DOX above 9.2 μM, embryos were reduced in body size, had deformed head with malformed eyes and otoliths/otocysts, malformed notochord and scoliosis. The muscle disintegration, accompanied with reduced caudal circulation, was particularly observable under 92 μM DOX, much more than under 92 μM FNP/DOX (results not shown).

Over the last few years zebrafish embryos have frequently been used as a reliable *in vivo* model for the bio-safety evaluation of diverse anticancer nanosystems.[2,24] The production of large number of embryos, rapid early embryonal development, and embryos/larvae transparency make zebrafish a particularly suitable model in toxicological and preclinical studies.[26]

In our study, embryos treated with 92 μM and 46 μM FNP/DOX had a significantly higher survival rate and lesser disturbance of cardiac functions than the embryos treated with the same dose of DOX alone, suggesting decreased overall toxicity of the nanocomposite in comparison to DOX. Toxic effects of DOX and FNP on the zebrafish embryos have previously been reported.[61,62] The cardiotoxicity of doxorubicin is among the main obstacles limiting its long-lasting therapeutic application,[63] and similarly, the pericardial edema was among the major adverse effects caused at DOX-treated zebrafish embryos.[62] In this study, we have demonstrated that a nanocomposite DOX/FNP induced the edema of pericardium to a significantly lesser extent than DOX alone. We have also demonstrated that it disturbed the heart beating rate, thus confirming a decreased cardiotoxicity and an increased safety of FNP/DOX as compared to DOX, which is a major challenge in the oncological practice where DOX is applied to the cancer patients.

Conclusion

In conclusion, DOX-loaded FNP was successfully made as a novel drug delivery system for cancer treatment. Self-assembling properties of fullerenol nanoparticles were used

Published on 14 April 2016. Downloaded by National Library of Serbia on 13/03/2018 11:39:29.

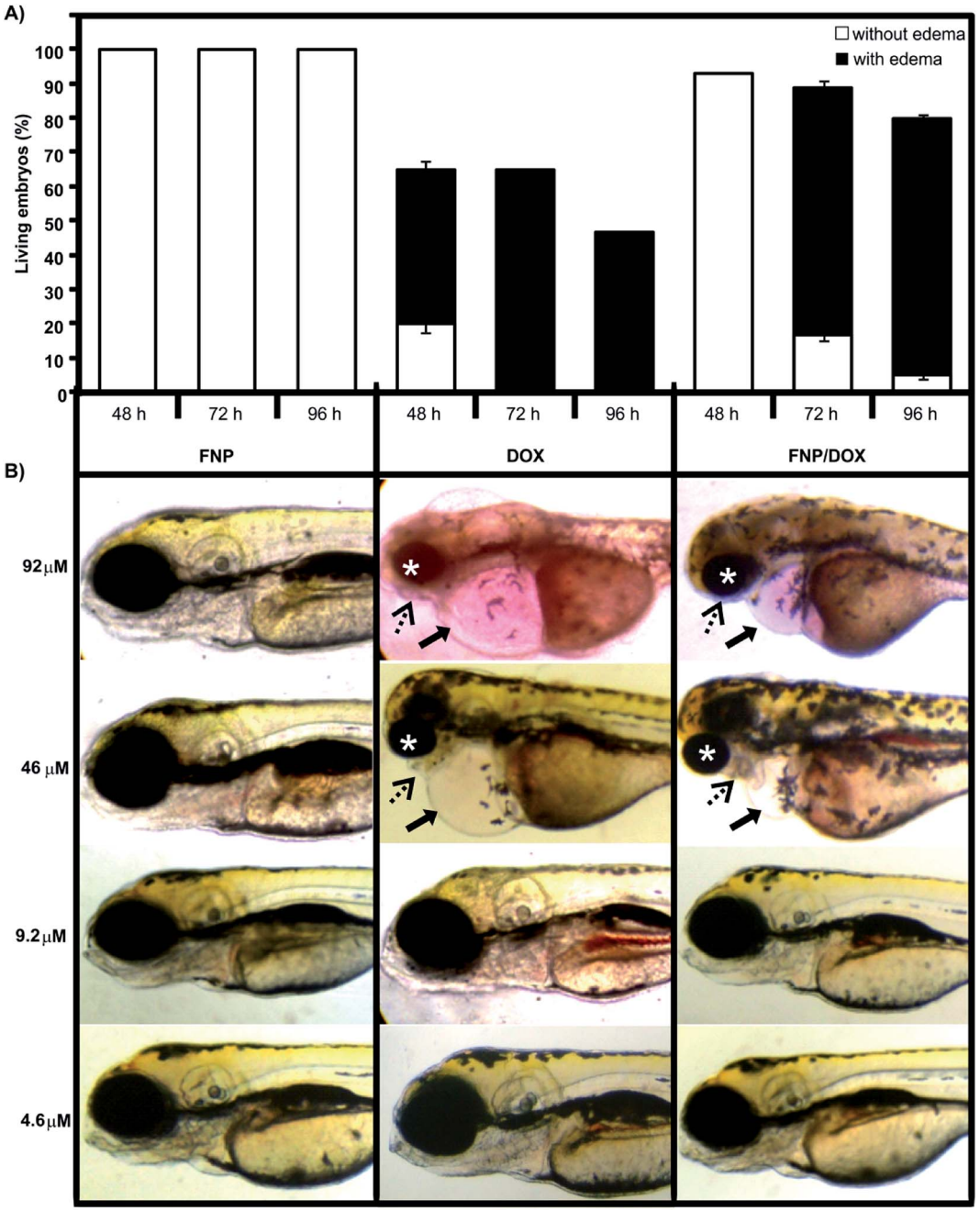

Fig. 13 Effects of FNP, DOX and FNP/DOX on the survival and the development of pericardial edema from 48–96 hpf in survived zebrafish embryos exposed to 46 μM of each substance (A). Images represent a dose-dependent effect of the tested substances on embryo morphology and severity of pericardial edema at 96 hpf (B). Pericardial edema (arrow), reduced jaw (dashed arrow) and malformed head and eyes (asterisk) are denoted.

for the formation of the FNP/DOX nanocomposite with commercial drug Adriablastin®. Simple preparation method of the nanocomposite indicates its potentially easy applicability in clinical practice. This nanocomposite system possesses small particle size (approximately 100 nm) and good stability. The FNP/DOX nanocomposite exhibited significantly enhanced cellular uptake and achieved remarkable cytotoxicity effects in MCF-7 and MDA-MB-231 cell lines. Moreover, the FNP/DOX nanocomposite significantly decreases breast cancer cells proliferation causing increase in DNA damage. Furthermore, zebrafish embryotoxicity assay showed decreased overall toxicity and increased safety of the nanocomposite in comparison to doxorubicin applied alone, which was manifested by the higher survival rate of embryos and less pericardial edema. The results of this research demonstrated that DOX-loaded FNP might be a potential drug-targeting delivery platform for cancer treatment. In future experiments the focus of our research will be on different *in vivo* healthy and tumor models.

 This journal is © The Royal Society of Chemistry 2016

Published on 14 April 2016. Downloaded by National Library of Serbia on 13/03/2018 11:39:29.

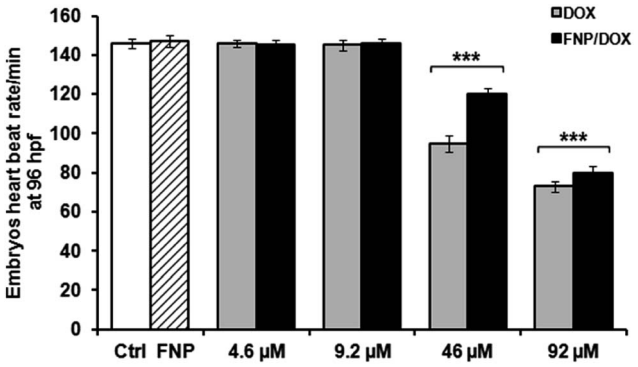

Fig. 14 Heart beat rate of the zebrafish embryos after the 96 h exposure to different concentrations of DOX and FNP/DOX. Embryos exposed to 8.9 μM FNP (corresponding to FNP concentration in 92 μM FNP/DOX) as well as to DOX and FNP/DOX in concentrations of 4.6 μM and 9.2 μM, did not differ in heart beating rate when compared to untreated embryos (Ctrl). *$P < 0.05$, **$P < 0.01$, ***$P < 0.001$.

Conflict of interest

The authors report no conflicts of interest in this work.

Acknowledgements

This work has received a financial support from the Ministry of Education and Science, Republic of Serbia, Grant No. III 45005 and 173048. We thank professor Alenka Mertelj (Institut "Jozef Stefan", Ljubljana, Slovenija) for DLS measurements. We also thank professor Vladimir Srdić (Faculty of Technology, University of Novi Sad, Serbia) for the zeta potential measurements.

References

1 J. L. Reeve, E. Szegezdi, S. E. Logue, T. N. Chonghaile, T. O'Brien, T. Ritter and A. Samali, *J. Cell. Mol. Med.*, 2007, **11**, 509–520.
2 P. Ma and R. J. Mumper, *Nano Today*, 2013, **8**, 313–331.
3 J. Li, Y. Wang, Y. Zhu and D. Oupicky, *J. Controlled Release*, 2013, **172**, 589–600.
4 F. Yang, S. S. Teves, C. J. Kemp and S. Henikoff, *Biochim. Biophys. Acta, Rev. Cancer*, 2014, **1845**, 84–89.
5 M. T. Tomicic and B. Kaina, *Biochim. Biophys. Acta, Rev. Cancer*, 2013, **1835**, 11–27.
6 Y.-L. Chang, H.-J. Lee, S.-T. Liu, Y.-S. Lin, T.-C. Chen, T.-Y. Hsieh, H.-S. Huang and S.-M. Huang, *Int. J. Biochem. Cell Biol.*, 2011, **43**, 1720–1728.
7 D. Giustarini, I. Dalle-Donne, D. Tsikas and R. Rossi, *Crit. Rev. Clin. Lab. Sci.*, 2009, **46**, 241–281.
8 A. Gudjoncik, C. Guenancia, M. Zeller, Y. Cottin, C. Vergely and L. Rochette, *Mol. Nutr. Food Res.*, 2014, **58**, 1721–1738.
9 C. Zhang and F. Zhang, *Protein Cell*, 2015, **6**, 88–100.
10 K. L. Malisza and B. B. Hasinoff, *Arch. Biochem. Biophys.*, 1995, **321**, 51–60.
11 E. Martin, A. V. Thougaard, M. Grauslund, P. B. Jensen, F. Bjorkling, B. B. Hasinoff, J. Tjørnelund, M. Sehested and L. H. Jensen, *Toxicology*, 2009, **255**, 72–79.
12 Y.-I. Jeong, S.-G. Jin, I.-Y. Kim, J. Pei, M. Wen, T.-Y. Jung, K.-S. Moon and S. Jung, *Colloids Surf., B*, 2010, **79**, 149–155.
13 Y.-H. Jin, H.-Y. Hu, M.-X. Qiao, J. Zhu, J.-W. Qi, C.-J. Hu, Q. Zhang and D.-W. Chen, *Colloids Surf., B*, 2012, **94**, 184–191.
14 J. A. Smith, L. Mathew, M. Burney, P. Nyshadham and R. L. Coleman, *Gynecol. Oncol.*, 2016, DOI: 10.1016/j.ygyno.2016.02.033.
15 S. K. Soininen, J. K. Repo, V. Karttunen, S. Auriola, K. H. Vähäkangas and M. Ruponen, *Toxicol. Lett.*, 2015, **239**, 108–114.
16 P. P. Wibroe, D. Ahmadvand, M. A. Oghabian, A. Yaghmur and S. M. Moghimi, *J. Controlled Release*, 2016, **221**, 1–8.
17 S. Zhu, M. Hong, G. Tang, L. Qian, J. Lin, Y. Jiang and Y. Pei, *Biomaterials*, 2010, **31**, 1360–1371.
18 R. Li, R. Wu, L. Zhao, M. Wu, L. Yang and H. Zou, *ACS Nano*, 2010, **4**, 1399–1408.
19 P. Chaudhuri, A. Paraskar, S. Soni, R. A. Mashelkar and S. Sengupta, *ACS Nano*, 2009, **3**, 2505–2514.
20 J.-H. Liu, L. Cao, P. G. Luo, S.-T. Yang, F. Lu, H. Wang, M. J. Meziani, S. A. Haque, Y. Liu and S. Lacher, *ACS Appl. Mater. Interfaces*, 2010, **2**, 1384–1389.
21 G. Bogdanović, V. Kojić, A. Đorđević, J. Čanadanović-Brunet, M. Vojinović-Miloradov and V. V. Baltić, *Toxicol. In Vitro*, 2004, **18**, 629–637.
22 S. Vandghanooni and M. Eskandani, *BioImpacts*, 2011, **1**, 87–97.
23 L. Gonzalez, B. Sanderson and M. Kirsch-Volders, *Mutagenesis*, 2011, **26**, 185–191.
24 S. L. Harper, J. L. Carriere, J. M. Miller, J. E. Hutchison, B. L. Maddux and R. L. Tanguay, *ACS Nano*, 2011, **5**, 4688–4697.
25 C.-W. Liu, F. Xiong, H.-Z. Jia, X.-L. Wang, H. Cheng, Y.-H. Sun, X.-Z. Zhang, R.-X. Zhuo and J. Feng, *Biomacromolecules*, 2013, **14**, 358–366.
26 N. S. Sipes, S. Padilla and T. B. Knudsen, *Birth Defects Res., Part C*, 2011, **93**, 256–267.
27 A. Djordjević, M. Vojinović-Miloradov, N. Petranović, A. Devečerski, D. Lazar and B. Ribar, *Fullerene Sci. Technol.*, 1998, **6**, 689–694.
28 S. M. Mirkov, A. N. Djordjevic, N. L. Andric, S. A. Andric, T. S. Kostic, G. M. Bogdanovic, M. B. Vojinovic-Miloradov and R. Z. Kovacevic, *Nitric Oxide*, 2004, **11**, 201–207.
29 A. AC03326419, *Cytogenetic analysis for radiation dose assessment: a manual*, Internat. Atomic Energy Agency, 2001.
30 M. Kirsch-Volders, T. Sofuni, M. Aardema, S. Albertini, D. Eastmond, M. Fenech, M. Ishidate, S. Kirchner, E. Lorge and T. Morita, *Mutat. Res., Genet. Toxicol. Environ. Mutagen.*, 2003, **540**, 153–163.
31 Organisation de coopération et de développement économiques, *Test No. 236: Fish Embryo Acute Toxicity (FET) Test*, OECD Publishing, 2013.
32 S. M. Cutts, A. Nudelman, A. Rephaeli and D. R. Phillips, *IUBMB Life*, 2005, **57**, 73–81.

Published on 14 April 2016. Downloaded by National Library of Serbia on 13/03/2018 11:39:29.

33 C. F. Thorn, C. Oshiro, S. Marsh, T. Hernandez-Boussard, H. McLeod, T. E. Klein and R. B. Altman, *Pharmacogenet. Genomics*, 2011, **21**, 440.
34 O. Tacar, P. Sriamornsak and C. R. Dass, *J. Pharm. Pharmacol.*, 2013, **65**, 157–170.
35 D. Goren, A. T. Horowitz, D. Tzemach, M. Tarshish, S. Zalipsky and A. Gabizon, *Clin. Cancer Res.*, 2000, **6**, 1949–1957.
36 R. C. Hui, R. E. Francis, S. K. Guest, J. R. Costa, A. R. Gomes, S. S. Myatt, J. J. Brosens and E. W. Lam, *Mol. Cancer Ther.*, 2008, **7**, 670–678.
37 I. Lentacker, B. Geers, J. Demeester, S. C. De Smedt and N. N. Sanders, *Mol. Ther.*, 2010, **18**, 101–108.
38 A. L. Seynhaeve, B. M. Dicheva, S. Hoving, G. A. Koning and T. L. Ten Hagen, *J. Controlled Release*, 2013, **172**, 330–340.
39 R. Injac, M. Perse, N. Obermajer, V. Djordjevic-Milic, M. Prijatelj, A. Djordjevic, A. Cerar and B. Strukelj, *Biomaterials*, 2008, **29**, 3451–3460.
40 R. Injac, M. Perse, M. Cerne, N. Potocnik, N. Radic, B. Govedarica, A. Djordjevic, A. Cerar and B. Strukelj, *Biomaterials*, 2009, **30**, 1184–1196.
41 S. Assemi, S. Tadjiki, B. C. Donose, A. V. Nguyen and J. D. Miller, *Langmuir*, 2010, **26**, 16063–16070.
42 B. Vileno, P. R. Marcoux, M. Lekka, A. Sienkiewicz, T. Fehér and L. Forró, *Adv. Funct. Mater.*, 2006, **16**, 120–128.
43 A. Albanese, P. S. Tang and W. C. Chan, *Annu. Rev. Biomed. Eng.*, 2012, **14**, 1–16.
44 S. W. Shin, I. H. Song and S. H. Um, *Nanomaterials*, 2015, **5**, 1351–1365.
45 M. A. Dobrovolskaia, P. Aggarwal, J. B. Hall and S. E. McNeil, *Mol. Pharmaceutics*, 2008, **5**, 487–495.
46 A. N. Ilinskaya and M. A. Dobrovolskaia, *Nanomedicine*, 2013, **8**, 773–784.
47 R. F. Greene, J. M. Collins, J. F. Jenkins, J. L. Speyer and C. E. Myers, *Cancer Res.*, 1983, **43**, 3417–3421.
48 B. D. Chithrani and W. C. Chan, *Nano Lett.*, 2007, **7**, 1542–1550.
49 W. Jiang, B. Y. Kim, J. T. Rutka and W. C. Chan, *Nat. Nanotechnol.*, 2008, **3**, 145–150.
50 B. Fubini, M. Ghiazza and I. Fenoglio, *Nanotoxicology*, 2010, **4**, 347–363.
51 G. D. Nielsen, M. Roursgaard, K. A. Jensen, S. S. Poulsen and S. T. Larsen, *Basic Clin. Pharmacol. Toxicol.*, 2008, **103**, 197–208.
52 X. Dai, Z. Yue, M. E. Eccleston, J. Swartling, N. K. Slater and C. F. Kaminski, *Nanomedicine*, 2008, **4**, 49–56.
53 K. K. Upadhyay, A. N. Bhatt, A. K. Mishra, B. S. Dwarakanath, S. Jain, C. Schatz, J.-F. Le Meins, A. Farooque, G. Chandraiah and A. K. Jain, *Biomaterials*, 2010, **31**, 2882–2892.
54 A. Zou, M. Huo, Y. Zhang, J. Zhou, X. Yin, C. Yao, Q. Zhu, M. Zhang, J. Ren and Q. Zhang, *J. Pharm. Sci.*, 2012, **101**, 627–640.
55 R. Lüpertz, W. Wätjen, R. Kahl and Y. Chovolou, *Toxicology*, 2010, **271**, 115–121.
56 E.-J. Park, H.-K. Kwon, Y.-M. Choi, H.-J. Shin and S. Choi, *PLoS One*, 2012, **7**, e44990.
57 N. Rusetskaya, N. Y. Lukyanova and V. Chekhun, *Exp. Oncol.*, 2009, **31**, 140–143.
58 J. A. Kim, C. Åberg, A. Salvati and K. A. Dawson, *Nat. Nanotechnol.*, 2012, **7**, 62–68.
59 J. Mrđanović, S. Šolajić, V. Bogdanović, K. Stankov, G. Bogdanović and A. Djordjevic, *Mutat. Res., Genet. Toxicol. Environ. Mutagen.*, 2009, **680**, 25–30.
60 J. Mrđanovic, S. Šolajić, V. Bogdanović, A. Đorđević, G. Bogdanović, R. Injac and Z. Rakočević, *J. Nanomater. Biostruct.*, 2012, **7**, 673–686.
61 C. Y. Usenko, S. L. Harper and R. L. Tanguay, *Carbon*, 2007, **45**, 1891–1898.
62 Y. Han, J. P. Zhang, J. Q. Qian and C. Q. Hu, *J. Appl. Toxicol.*, 2015, **35**, 241–252.
63 S. M. Swain, F. S. Whaley and M. S. Ewer, *Cancer*, 2003, **97**, 2869–2879.

 This journal is © The Royal Society of Chemistry 2016